Quantification of Regional Ventilation–Perfusion Ratios with PET

Marcos F. Vidal Melo, MD, PhD[1]; Dominick Layfield, MSc[2]; R. Scott Harris, MD[3]; Kevin O'Neill, MSc[2]; Guido Musch, MD[1]; Torsten Richter, MD[4]; Tilo Winkler, PhD[1]; Alan J. Fischman, MD, PhD[5]; and Jose G. Venegas, PhD[1]

[1]Department of Anesthesia and Critical Care, Massachusetts General Hospital and Harvard Medical School, Boston, Massachusetts; [2]School of Engineering, Massachusetts Institute of Technology, Boston, Massachusetts; [3]Pulmonary and Critical Care Unit, Department of Medicine, Massachusetts General Hospital and Harvard Medical School, Boston, Massachusetts; [4]Clinic of Anesthesiology and Intensive Care Medicine, University Clinic Carl Gustav Carus, Dresden University of Technology, Dresden, Germany; and [5]Department of Radiology, Massachusetts General Hospital and Harvard Medical School, Boston, Massachusetts

The topographic matching of alveolar ventilation ($\dot{V}_A$) and perfusion ($\dot{Q}$) is the main determinant of gas exchange efficiency of the lung. However, no pulmonary functional imaging technique has been shown to predict whole-lung gas exchange in health and disease. This study aims to present a PET-based method to estimate regional alveolar ventilation-to-perfusion ratios ($\dot{V}_A/\dot{Q}$) predictive of arterial blood gases. **Methods:** The method is based on the regional tracer kinetics of ^{13}N-nitrogen (^{13}NN) after an intravenous bolus injection during a breath-hold period and subsequent washout from the lungs with resumption of breathing. The method takes into account the presence of inter- and intraregional nonuniformities at length scales smaller than the imaging spatial resolution. An algorithm used regional tracer washout to classify regional $\dot{V}_A/\dot{Q}$ uniformity. Intraregional $\dot{V}_A/\dot{Q}$ mismatch in nonuniform regions was described with a 2-compartment model. Regional $\dot{V}_A/\dot{Q}$ estimates were combined into a whole-lung distribution of $\dot{V}_A/\dot{Q}$ ratios and were used to compute global arterial blood gases. The method was applied to 3-dimensional PET data from anesthetized and mechanically ventilated sheep before and after methacholine bronchoconstriction ($n = 3$) and pulmonary embolism ($n = 3$) and after saline lung lavage ($n = 3$). **Results:** PET images revealed regional changes in ventilation and perfusion consistent with the different disease models. Quantification of the images using PET-derived $\dot{V}_A/\dot{Q}$ distributions showed unimodal and narrow distributions in control conditions that became wider and unimodal after pulmonary embolism and saline lung lavage and bimodal after bronchoconstriction. Images of regional gas exchange allowed for visualization of regional gas exchange. Arterial blood gases estimated from the PET-based $\dot{V}_A/\dot{Q}$ distributions closely agreed with measured values (partial pressure of oxygen, arterial [Pa_{O_2}]: $r^2 = 0.97$, $P < 0.001$; partial pressure of carbon dioxide, arterial [Pa_{CO_2}]: $r^2 = 0.96$, $P < 0.001$). **Conclusion:** Tracer kinetics analysis of PET images after an intravenous injection of ^{13}NN provides a quantitative assessment of regional $\dot{V}_A/\dot{Q}$ heterogeneity including that corresponding to length scales smaller than the spatial resolution of the imaging method. Quantification of $\dot{V}_A/\dot{Q}$ mismatch obtained with the presented technique is directly related to severity of gas exchange impairment as determined by arterial blood gases.

Key Words: lung; mathematic model; PET; sheep; ventilation–perfusion

J Nucl Med 2003; 44:1982–1991

The topographic matching of alveolar ventilation ($\dot{V}_A$) and perfusion ($\dot{Q}$) is the main determinant of gas exchange efficiency of the lung. For this reason, techniques were developed to quantify the distribution of $\dot{V}_A/\dot{Q}$ ratios. Traditional approaches involved the estimation of $\dot{V}_A/\dot{Q}$ from whole-lung gas exchange data, such as concentrations of respiratory or inert gases in expired air or in blood samples (*1*,*2*), yielding no topographic information. One of these functional approaches, the multiple inert gas elimination technique (MIGET) (*2*), is the most frequently used for quantification of $\dot{V}_A/\dot{Q}$ distributions.

In addition, methods based on inhaled or infused tracers have been developed to image the topographic distribution of $\dot{V}_A$, $\dot{Q}$, and $\dot{V}_A/\dot{Q}$. Initial studies were performed with planar ventilation–perfusion scans (*3*,*4*). In spite of the limited 3-dimensional information of planar scintigraphy, clinical studies based on this technique demonstrated the value of quantitative analysis of lung imaging for diagnosis of pulmonary embolism (*5*) and pathophysiologic investigation of chronic obstructive pulmonary disease (*6*). More recently, imaging methods that provide enhanced 3-dimensional information on pulmonary $\dot{V}_A$, $\dot{Q}$, and $\dot{V}_A/\dot{Q}$ have become available: MRI of inhaled hyperpolarized ^{3}He (*7*), oxygen and gadopentetate dimeglumine (*8*) or sulfur hexafluoride (*9*), CT images of xenon washin (*10*), SPECT of aerosolized ^{99m}Tc-diethylenetriaminepentacetate followed by perfusion tomography after injection of ^{99m}Tc-labeled macroagregated albumin (*11*,*12*), and PET of inhaled or injected ^{13}N-nitrogen (^{13}NN) (*13–16*). However, none of these techniques has been shown to be capable of

Received Apr. 8, 2003; revision accepted Sep. 8, 2003.

For correspondence or reprints contact: Marcos F. Vidal Melo, MD, PhD, Cardiac Anesthesia Group, Department of Anesthesia and Critical Care, Massachusetts General Hospital, 55 Fruit St., Boston, MA 02114.

E-mail: mvidalmelo@partners.org

predicting whole-lung gas exchange. Demonstration of such capability in disease conditions would imply that the functional imaging technique would be able to quantify the main determinant of gas exchange in addition to providing topographic information.

In this article, we present a PET-based method to assess regional $\dot{V}_A/\dot{Q}$ using the distribution and elimination kinetics of ^{13}NN from the lungs after an intravenous injection of the tracer in saline solution. The method is validated in data from mechanically ventilated sheep before and after pulmonary embolism, acute lung injury with saline lung lavage, and bronchoconstriction.

MATERIALS AND METHODS

Animal Preparation

The experimental protocols were approved by the Committee on Animal Care of our institution. Nine sheep weighing 23 ± 6 kg were studied: 3 before and after autologous blood clot pulmonary embolism, 3 after saline lung lavage, and 3 before and after methacholine-induced bronchoconstriction. The animals were anesthetized, intubated, and mechanically ventilated. General anesthesia was induced with an intravenous bolus of sodium thiopental and maintained with a continuous infusion of sodium thiopental and fentanyl. Pancuronium was used for muscle paralysis. The ventilator (Harvard Apparatus) was set at an inspired oxygen fraction (F_{IO_2}) = 0.24 for the pulmonary embolism protocol, 0.49 for the bronchoconstriction protocol, and 1.0 for the saline lung lavage protocol; positive end-expiratory pressure = 5 cm H_2O; tidal volume (V_T) = 15 mL/kg for bronchoconstriction and 8 mL/kg for pulmonary embolism and saline lung lavage; and inspiratory time of 30% of the breathing period. Respiratory rate (RR = 15 ± 4 bpm) was set to maintain normocapnic arterial blood gases at the beginning of the experiment and fixed at that value for the rest of the experiment. The right femoral artery was cannulated for systemic arterial pressure monitoring and blood sampling and the right femoral vein was cannulated for administration of drugs. A Swan–Ganz catheter (model 93A-131H-7F; Edwards Laboratory) was inserted in the left femoral vein and advanced into the pulmonary artery. Its distal port was used for monitoring of pulmonary arterial pressure (PAP) and sampling of pulmonary arterial blood. A central line was introduced in a jugular vein and positioned into the superior vena cava for delivery of the ^{13}NN-saline solution.

For the pulmonary embolism protocol, a second and larger (7-mm inner diameter) central line was introduced into the contralateral internal jugular vein and used for infusion of the autologous blood clots in the pulmonary embolism studies. Autologous clots were produced as described previously (*17*) in cylindric molds of equal height and diameter drilled on an acrylic board. Pulmonary embolism was induced by progressive infusion of eight 4- to 8-mm-diameter individual clots. The lung lavage studies had acute lung injury produced with bilateral warmed isotonic saline lung lavage (30 mL/kg) to remove lung surfactant. The solution was flushed in and out of the lungs and repeated after 5 min until a ratio of arterial O_2 partial pressure (Pa_{O_2}) to F_{IO_2} < 100 mm Hg was achieved. For the bronchoconstriction studies, methacholine solution (25 mg/mL) was delivered through the inspiratory line with an ultrasonic nebulizer. The methacholine dose was titrated in order to double the control peak airway pressure (P_{peak}).

Physiologic Measurements

The following physiologic variables were measured: (a) Cardiovascular: heart rate (HR), invasive systemic blood pressure, PAP, pulmonary artery occlusion pressure (PAOP), and cardiac output (CO); (b) Respiratory: V_T, RR, F_{IO_2}, P_{peak}, partial pressures of O_2 and CO_2 in the arterial (Pa_{O_2}, Pa_{CO_2}) and mixed venous (Pv_{O_2}, Pv_{CO_2}) blood, end-tidal P_{CO_2} (Pet_{CO_2}), and mixed-expired P_{CO_2}. Alveolar ventilation was computed as $\dot{V}_A = (V_T - V_D)\cdot RR$, where V_D = dead space was estimated from the animal's weight (*18*). Physiologic measurements were performed within 10 min of PET measurements.

PET Imaging Protocol and Processing

The experimental apparatus included a PET camera and a tracer infusion system. A Scanditronix PC4096 multiring whole-body PET camera (General Electric Medical Systems) was used in the stationary mode. The infusion system consisted of a computer-controlled device for production and injection of the ^{13}NN-saline solution. The tracer ^{13}NN gas (~10-min half-life) was generated by a cyclotron and dissolved in degassed saline, yielding a specific activity of 14.4 ± 6.7 MBq/mL. A bolus of ^{13}NN-saline (20–30 mL) was injected into a central vein at a rate of 10 mL/s under computer control.

The animal was positioned in the camera field with the most caudal slice adjacent to the diaphragm dome. Animals were prone for the normal, bronchoconstriction, and pulmonary embolism studies and supine for the lung lavage study. The PET camera collected 15 transverse cross-sectional slices of 6.5-mm thickness providing 3-dimensional information over a 9.7-cm-long cylinder. Based on the ratio between the maximal injected activity in the lung field and the total injected activity, we estimate that the imaged lung corresponded to ~70% of the total lung volume. Transmission scans were obtained before each set of emission scans to correct for absorption of annihilation photons in the animal's body and to delimit the regions of interest (ROIs) corresponding to lung fields. Transmission scans were obtained by imaging the lung for 10 min, while a linear rod source of ^{68}Ge rotated around the body.

The imaging protocol for the emission scans was as follows: Starting with a tracer-free lung, the ventilator was turned off at the end of exhalation and a bolus of ^{13}NN-saline solution (~300 MBq) was injected into a central vein. Simultaneously, collection of consecutive images was started, while the animal was kept in apnea for 60 s. At the end of these 60 s, mechanical ventilation was resumed and the lungs were imaged as the tracer washed out of the lungs. The imaging sequence for the pulmonary embolism and lung lavage experiments during the apneic phase consisted of 8 images of 2.5 s and 4 images of 10 s and during the washout phase consisted of 6 images of 10 s and 4 images of 30 s. For the bronchoconstriction studies, the imaging sequence during the apneic phase consisted of 6 images of 10 s and during the washout phase consisted of 4 images of 30 s and 2 images of 60 s. A sample of the infusate was collected to assess its specific activity in a well counter cross-calibrated with the PET camera.

Emission scans were reconstructed with appropriate correction for detector sensitivity and for tissue attenuation using a convolution backprojection algorithm with a Hanning filter, yielding an effective spatial resolution of 6 mm (determined from the width at one-half height of a point source image). Resulting images consisted of an interpolated matrix of 128 × 128 × 15 voxels of 6 × 6 × 6.5 mm. To reduce imaging noise, images were low-pass

filtered to 13 × 13 mm in the image plane and a 2-point moving average filter was applied in the z-plane to a final volumetric resolution of ~2.2 cm^3. These filtered raw images were processed following the methodology described below to generate functional images. Transmission and emission scans were obtained before and after induction of bronchoconstriction and pulmonary embolism and after saline lung lavage.

Theory for Analysis of Regional Tracer Kinetics

The computation of regional $\dot{V}_A/\dot{Q}$ was derived from PET-imaged regional pulmonary kinetics of ^{13}NN after an intravenous injection of the tracer during a short apnea and subsequent washout period. Given the extremely low solubility of nitrogen in blood and tissues (partition coefficient $\lambda = 0.018$) and the associated minimal diffusional resistance of the alveolar capillary membrane to nitrogen (*13*), after an intravenous injection of ^{13}NN-saline solution, virtually all ^{13}NN in the blood diffuses into alveolar gas spaces at the first pass in aerated lung units. If the lungs are kept apneic during and after tracer arrival, tracer content, and thus regional radioactivity measured with PET, remains nearly constant in these aerated units and is therefore proportional to regional pulmonary blood flow ($\dot{Q}r$)—that is, the pulmonary blood flow in a specific ROI. In this work, this ROI corresponded to a voxel. Once ventilation is resumed, the tracer is washed out from the lungs (Fig. 1A). In the case of uniform intraregional ventilation distribution, the regional tracer activity (A(t)) after correction for radioactive tracer decay is:

$$A(t) = A_0 \cdot e^{-t/\tau}, \qquad \text{Eq. 1}$$

where A_0, the activity of the tracer at the beginning of the washout, is proportional to regional perfusion ($A_0 = k \cdot \dot{Q}r$).

The inverse of the time constant τ is equal to the regional specific ventilation ($s\dot{V}_r$) or ventilation per unit volume. The integral of Equation 1 during washout from t = 0 to ∞ can be rewritten as:

$$\int_0^\infty A(t)dt = \int_0^\infty A_0 \cdot e^{-t/\tau} dt = A_0 \cdot \tau = k \cdot \dot{Q}r/s\dot{V}r, \qquad \text{Eq. 2}$$

where k is the proportionality constant. It follows that for uniform intraregional ventilation, the integral of regional activity imaged during the tracer washout is proportional to $\dot{Q}_r/s\dot{V}_r$.

In the case of nonuniform intraregional $\dot{V}_A/\dot{Q}$ distribution, the kinetics of regional activity can be approximated by a biexponential washout (Fig. 1B):

$$A(t) = A_{0f} \cdot e^{-t/\tau_f} + A_{0s} \cdot e^{-t/\tau_s}, \qquad \text{Eq. 3}$$

where the indices f and s refer to a fast and a slow compartment and A_{0f} and A_{0s} are the activities in each of these compartments at the beginning of the washout. In this case, the integral of A(t) corresponds to the sum of the integrals for each compartment: $A_{0f} \cdot \tau_f = k \cdot (\dot{Q}_r/s\dot{V}_r)_f$ and $A_{0s} \cdot \tau_s = k \cdot (\dot{Q}_r/s\dot{V}_r)_s$. From Equation 3 evaluated at t = 0, the total regional activity before the washout is $A_0 = A_{0f} + A_{0s}$, where A_{0s} can be estimated in a semilogarithmic plot by fitting a line to the late part of the washout and extrapolating to the time at the beginning of the washout (Fig. 1B).

A limit case arises when the slope of the slow compartment washout tends to zero ($\tau_s \to \infty$). This corresponds to a perfused compartment with essentially no ventilation and finite regional volume as it would occur with gas trapping during bronchoconstriction. In this case, since $\dot{V}_A \approx 0$ and regional perfusion is finite, $\dot{V}_A/\dot{Q} \approx 0$.

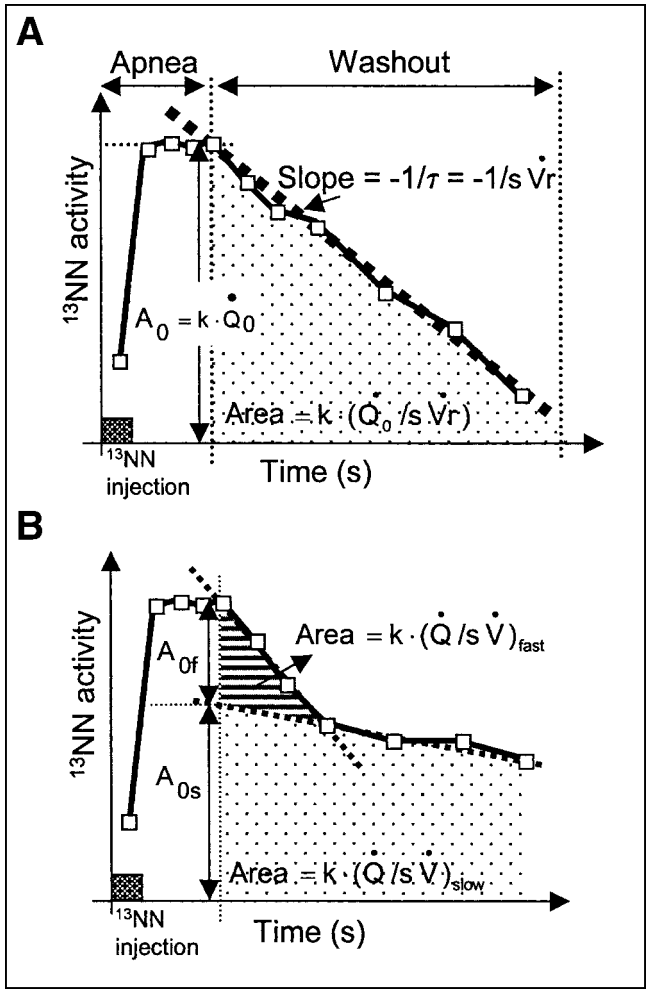

FIGURE 1. (A) Semilogarithmic plot of voxel ^{13}NN activity vs. time in voxel exhibiting uniform (1 compartment) behavior. Initial activity A_0 is proportional to regional perfusion $\dot{Q}_0$. Washout time constant τ corresponds to inverse of regional specific ventilation ($s\dot{V}r$). Thus, area under curve is given by $A_0 \cdot \tau = k \cdot \dot{Q}_0/s\dot{V}r$—that is, proportional to ratio of perfusion to specific ventilation. (B) Semilogarithmic plot of voxel ^{13}NN activity vs. time for voxel exhibiting 2-compartment behavior. Tracer washout shows fast compartment with initial activity A_{0f} proportional to its respective initial perfusion $\dot{Q}_{fast}$ and slow compartment with initial activity A_{0s} proportional to its initial perfusion $\dot{Q}_{slow}$. Hatched and dotted areas indicate values of $k \cdot \dot{Q}/s\dot{V}r$ corresponding to each of those compartments.

Regional Perfusion

As described above in Theory, the average regional tracer activity measured in the images collected during the plateau phase of apnea ($\bar{A}_{plateau}$) is proportional to $\dot{Q}_r$. An image of relative regional perfusion ($\dot{q}_r$) can be built as $\bar{A}_{plateau}$ divided by the total tracer activity over the whole imaged lung field (sum of $\bar{A}_{plateau}$ for all voxels). Absolute regional perfusion ($\dot{Q}_r$) was computed as $\dot{q}_r \cdot \dot{Q}_p$, where $\dot{Q}_p$ = pulmonary blood flow computed as described in Computation of Regional $\dot{V}_A/\dot{Q}$.

Algorithm for Analysis of Regional $\dot{V}_A/\dot{Q}$

Computation of regional $\dot{V}_A/\dot{Q}$ was based on the tracer kinetics at the voxel level. The method is related to the hybrid method used to describe intraregional ventilatory nonuniformities after tracer inhalation (*19*). A voxel classification algorithm was used to define the method of analysis for each voxel. It was based on the mean voxel activity during the last 3 images of the washout ($\bar{A}_{end}$) and the respective rate of washout during these images (α_{end}). Calling A_0 the tracer activity at the beginning of the washout, each voxel was classified in 1 of 3 groups:

1. $\bar{A}_{end} < 0.1 \cdot A_0$: In this condition, most of the tracer is washed out at the end of the scanning period. In these voxels, data were analyzed as a 1-compartment system and the value of $k \cdot (\dot{Q}_r/s\dot{V}_r)$ was obtained as in Equation 2 using a numeric integration.
2. $\bar{A}_{end} \geq 0.1 \cdot A_0$ and $\alpha_{end} < 0$: In this condition, there is a substantial amount of residual tracer at the end of the washout. Voxel data were analyzed according to a 2-compartment system assuming that the fast compartment is mostly cleared within the first 90 s (*20*). The time constant of the slow compartment, τ_s, was computed as the rate of voxel washout during the last 3 images. A_{0s}, the tracer content of the slow compartment at the start of the washout phase, was estimated in a semilogarithmic plot by fitting a line to the last 3 points of the washout and extrapolating to the time at the beginning of the washout (Fig. 1B). Once τ_s and A_{0s} were known, $k \cdot \dot{Q}_r/s\dot{V}_r$ of the slow compartment was computed as $\tau_s \cdot A_{0s}$. The fraction of regional perfusion to the slow compartment was computed as A_{Os}/A_O. For the fast compartment, $k \cdot (\dot{Q}_r/s\dot{V}_r)$ was computed from Equation 3 as the total integral subtracted from $\tau_s \cdot A_{0s}$. The fraction of regional perfusion to the fast compartment was computed as $A_{Of}/A_O = (1 - A_{Os})/A_O$.
3. $\bar{A}_{end} \geq 0.1 \cdot A_0$ and $\alpha_{end} = 0$: In this case, a fraction of alveolar units within the voxel had zero ventilation but was aerated and perfused ($\dot{V}_A/\dot{Q} \approx 0$)—that is, there was gas trapping. We analyzed these areas as composed of 2 compartments: one corresponding to $\dot{V}_A/\dot{Q} = 0$ (shunt effect) and the other with a finite $\dot{V}_A/\dot{Q}$. The fraction of regional perfusion to the units with $\dot{V}_A/\dot{Q} = 0$ within a voxel was computed as the ratio between the average of the activities during the late washout plateau and the initial activity—that is, $\bar{A}_{end}/A_O$. The rest of the voxel perfusion was assigned to a finite $\dot{V}_A/\dot{Q}$ compartment with $k \cdot \dot{Q}_r/s\dot{V}_r$ computed by subtracting from the total numeric integral during the washout the component corresponding to the region with $\dot{V}_A/\dot{Q} = 0$.

Computation of Regional $\dot{V}_A/\dot{Q}$ and Global $\dot{V}_A/\dot{Q}$ Distributions

Regional compartment $s\dot{V}_r/(k \cdot \dot{Q}_r)$ was calculated as the inverse of $k \cdot \dot{Q}_r/s\dot{V}_r$. We assumed that specific ventilation $s\dot{V}_r$ was proportional to regional ventilation $\dot{V}_r$ and, thus, $s\dot{V}_r/\dot{Q}$ was proportional to $\dot{V}_A/\dot{Q}$. Implicit here is the assumption of uniform volume of distribution of the tracer gas, and hence a uniform alveolar unit volume, within the lung.

To generate distributions of $\dot{V}_A/\dot{Q}$ in absolute units, we used the physiologic measurements of $\dot{Q}_T$ and $\dot{V}_A$ and an estimate of the right-to-left shunt fraction ($\dot{Q}_S/\dot{Q}_T$). $\dot{Q}_S/\dot{Q}_T$ was estimated from the global tracer kinetics in the lung imaged field during the apneic phase according to a previously described method (*21*) added to the perfusion to regions with $\dot{V}_A/\dot{Q} = 0$ described above in Algorithm for Analysis of Regional $\dot{V}_A/\dot{Q}$ item 3.

We assumed that the regional distributions of ventilation and perfusion obtained from the imaged lung characterized those of the whole lung. Absolute perfusion for each compartment in each voxel was computed from the measurements of relative perfusion $\dot{q}_r$ as $f \cdot \dot{q}_r \cdot \dot{Q}_p = f \cdot \dot{Q}_r$, where f was the fraction of perfusion to the corresponding compartment, and pulmonary blood flow ($\dot{Q}_p$) was computed as $\dot{Q}_p = \dot{Q}_T \cdot (1 - \dot{Q}_S/\dot{Q}_T)$. Alveolar ventilation for each compartment in each voxel was computed in 2 steps. First, a value proportional to the compartment's ventilation was calculated as the product of the compartment's perfusion ($f \cdot \dot{Q}_r$) by the compartment's $\dot{V}_A/\dot{Q}$ ($s\dot{V}_r/(k \cdot \dot{Q}_r)$). Absolute ventilation for each compartment was then computed by adjusting these proportional ventilation values to the measured alveolar ventilation.

Selection of Voxels for Analysis

Selection of ROIs for the lung fields was created by thresholding the transmission scans. Images of $\dot{Q}_r$ obtained after pulmonary embolism and lung lavage were used to identify areas that remained perfused and, thus, participating in gas exchange after induction of lung injury.

Gas Exchange Computations

Each set of functional data contained between 17,000 and 40,000 voxels. To present the results and estimate gas exchange indices from the obtained distributions, regional $\dot{V}_A/\dot{Q}$ values were condensed into 100 bins of equal $\log(\dot{V}_A/\dot{Q})$ width (0.05) ranging from -3 to 2. Values under -3 (i.e., $\dot{V}_A/\dot{Q} < 10^{-3}$) were considered shunt, and values above 2 (i.e., $\dot{V}_A/\dot{Q} > 10^2$) were considered dead space. The square root of the second moment of the perfusion-weighted $\dot{V}_A/\dot{Q}$ distribution about its mean on a logarithmic scale (SD_Q) was used as an indicator of $\dot{V}_A/\dot{Q}$ heterogeneity (*22*).

Computation of Alveolar and Blood Gas Partial Pressures

Global alveolar and blood O_2 and CO_2 partial pressures were obtained by computing partial pressures and contents for each $\dot{V}_A/\dot{Q}$ bin through the solution of mass conservation equations for O_2, CO_2, and N_2 assuming alveolar–capillary gas diffusion equilibrium (*23*). Nonlinear oxygen dissociation curves for sheep as described by Sharan and Popel (*24*) and partial pressure versus content relationships for CO_2 as described by Loeppky et al. (*25*) were used. Mean alveolar partial pressures of O_2 and CO_2 were calculated as the average of the bins' O_2 and CO_2 partial pressures weighted by their relative ventilation. Global blood gas contents were calculated as an average of all bins weighted by their relative perfusion, including shunt. The corresponding blood partial pressures were computed using the dissociation curves.

Mapping of Regional Gas Exchange

Maps of regional end-capillary O_2 saturation (Sec_{O_2}) and CO_2 partial pressure (Pec_{CO_2}) were generated by color coding the computed values of Sec_{O_2} and Pec_{CO_2} derived from the estimated regional $\dot{V}_A/\dot{Q}$. In the voxels with 2-compartmental behavior, a perfusion-weighted value for Sec_{O_2} was used. To compute regional Pec_{CO_2} in these voxels, a perfusion-weighted Cec_{CO_2} was calculated and the corresponding Pec_{CO_2} was estimated from the P_{CO_2} versus content curve.

Statistical Analysis

Data are expressed as mean ± SD. Comparisons between values before and after bronchoconstriction or pulmonary embolism were made by using a 2-tailed Student *t* test for paired samples. SD_Q values after lung lavage were compared with control values by using a 2-tailed Student *t* test for unpaired samples. Linear correlation and biases (*26*) were used to summarize the relationship between the measured and estimated variables. Statistical significance was taken at $P < 0.05$ level.

RESULTS

Respiratory and hemodynamic changes consistent with each induced disease state were obtained after pulmonary embolism, lung lavage, and bronchoconstriction (Table 1). Correspondingly, emissions scans showed areas of no regional perfusion after pulmonary embolism, redistribution of perfusion after lung lavage, and high concentration of residual tracer at the end of washout images during bronchoconstriction (Fig. 2). These contrasted with the relatively homogeneous distribution of regional perfusion and nearly complete tracer elimination at the end of washout in normal sheep (Fig. 2).

Regional Tracer Kinetics

Different patterns of tracer kinetics were observed (Fig. 3). A large fraction of the lungs for the control sheep (97% ± 5%) and also for sheep after pulmonary embolism (90% ± 10%) presented single-compartment washouts (Fig. 3A). A small fraction of voxels during control and after pulmonary embolism (<1%) and a larger number of voxels after lung lavage (10% ± 12%) and bronchoconstriction (57% ± 15%) showed intraregional heterogeneity and were analyzed as 2 compartments (Fig. 3B). Also, a significant fraction of voxels after lung lavage (45% ± 24%) and bronchoconstriction (16% ± 4%) showed either partial (Fig. 3C) or virtually complete (Fig. 3D) intraregional gas trapping corresponding to zero ventilation (and, thus, $\dot{V}_A/\dot{Q} \approx 0$).

Gas Exchange Analysis

PET-derived distributions of $\dot{V}_A/\dot{Q}$ ratios in terms of fractional perfusion and ventilation during control conditions presented a unimodal narrow distribution (Fig. 2). Unimodal and wider $\dot{V}_A/\dot{Q}$ distributions were seen after pulmonary embolism and lung lavage (Fig. 2). Lung lavage animals presented right-to-left shunt fractions markedly larger than any other condition. The widest $\dot{V}_A/\dot{Q}$ distributions were measured during bronchoconstriction (Fig. 2). These distributions were consistently bimodal (Fig. 2) with substantial portions of the blood flow reaching areas of low $\dot{V}_A/\dot{Q}$. The second moment of the $\dot{V}_A/\dot{Q}$ distributions (SD_Q) increased from 0.14 ± 0.04 for the control sheep to 0.18 ± 0.05 ($P < 0.05$) in sheep after pulmonary embolism, 0.31 ± 0.03 ($P < 0.05$) after lung lavage, and 0.88 ± 0.30 ($P < 0.05$) after bronchoconstriction.

Pa_{O_2} and Pa_{CO_2} values estimated from PET-derived $\dot{V}_A/\dot{Q}$ distributions were highly correlated with direct measurements of arterial blood gases (Figs. 4 and 5). Estimates of Pa_{O_2} correlated with Pa_{O_2} measurements ($r^2 = 0.97$, $P < 0.001$) with regression equation Pa_{O_2} measured = 0.996·Pa_{O_2} estimated – 3.2 mm Hg (Fig. 4). The mean difference between

TABLE 1
Hemodynamic and Respiratory Data for Sheep Studied During Control Conditions and Induced Lung Dysfunction

Sheep	MAP (mm Hg)	MPAP (mm Hg)	CO (L/min)	F_{IO_2} (%)	P_{peak} (cm H_2O)	Pa_{O_2} (mm Hg)	Pa_{CO_2} (mm Hg)
Control							
1	90	14	2.6	48	17	276	38.7
2	120	13	2.7	49	20	300	34.5
3	80	12	3.0	49	23	291	37.7
4	104	17	2.9	22	19	98.6	39.7
5	120	28	4.2	26	22	126	35.0
6	108	16	3.6	25	22	103	35.9
BC							
1	50	18	2.4	48	49	53	47.1
2	60	15	2.2	48	50	59	36.3
3	80	15	3.1	48	42	157	43.6
PE							
4	100	21	3.0	22	21	88	39.0
5	108	30	4.2	26	24	106	39.0
6	106	18	4.2	25	24	106	37.9
LL							
7	42	16	3.3	100	26	48	33.3
8	62	20	4.1	100	29	62	59.2
9	108	16	3.5	100	35	126	49

MAP = mean arterial pressure; MPAP = mean pulmonary artery pressure; BC = bronchoconstriction; PE = pulmonary embolism; LL = saline lung lavage.

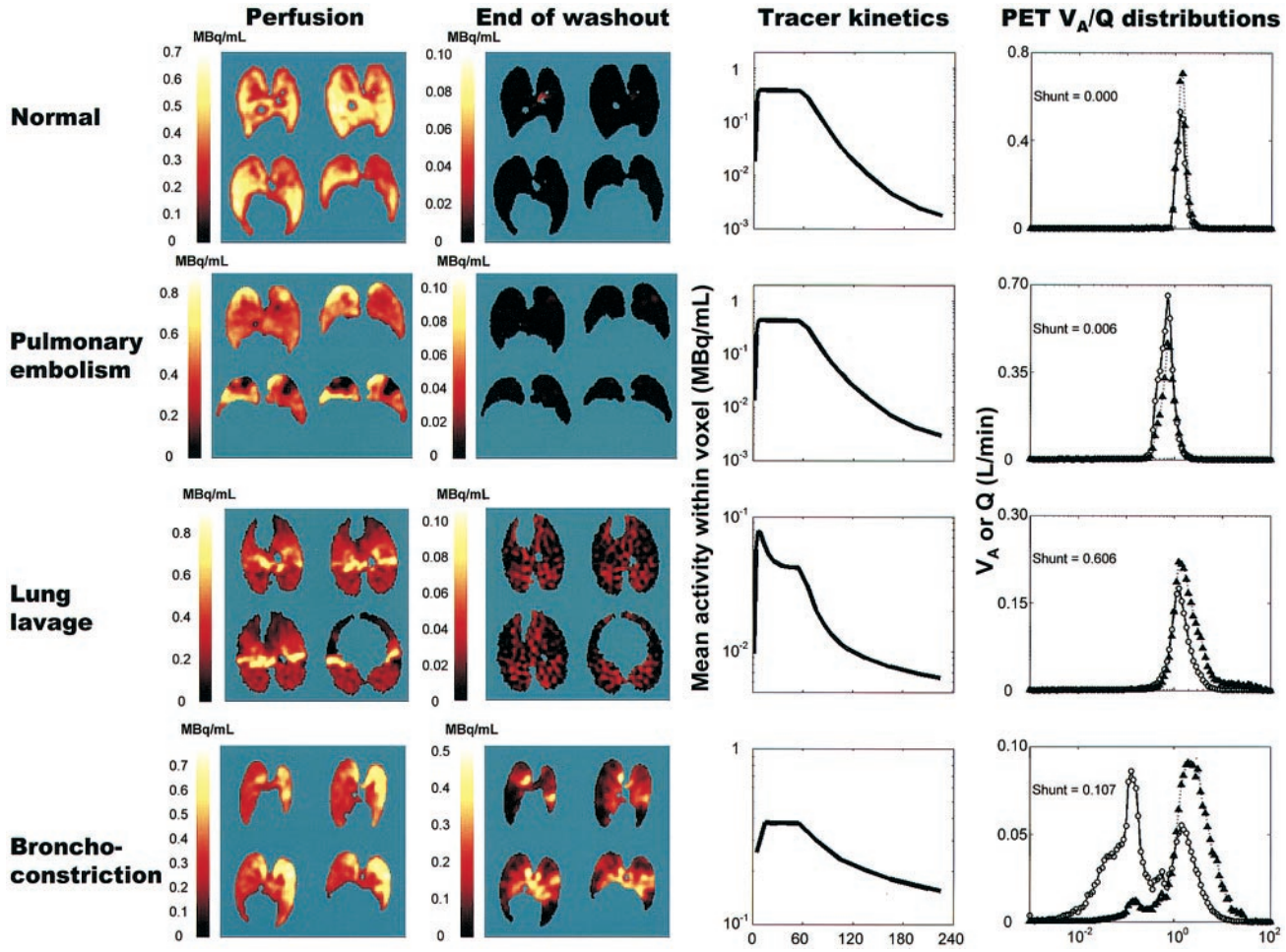

FIGURE 2. Regional perfusion and end-of-washout lung images, tracer kinetics of whole-lung field, and PET-derived $\dot{V}_A/\dot{Q}$ distributions for single examples of normal sheep and sheep after pulmonary embolism, saline lung lavage, and bronchoconstriction. Images are tomographic sections viewed in craniocaudal direction from top to bottom. Animals were prone for normal, bronchoconstriction, and pulmonary embolism studies and supine for lung lavage study. In supine position, left side in image corresponds to left side in animal. Note different scales for images. Regions of unperfused lung are seen after embolism. After lung lavage, there is redistribution of perfusion and increase in residual tracer at end of washout. Early peak and fast drop to plateau in lung lavage tracer kinetics indicates presence of intrapulmonary shunt. There is significant retention of tracer in large areas after bronchoconstriction.

measured and estimated Pa_{O_2} was 3.7 ± 15.3 mm Hg. Estimates of Pa_{CO_2} also correlated with measurements of Pa_{CO_2} ($r^2 = 0.96$, $P < 0.001$) with regression equation Pa_{CO_2} measured = 1.017·Pa_{CO_2} estimated + 0.6 mm Hg (Fig. 5). Estimates of Pa_{CO_2} approximated Pa_{CO_2} measurements with a mean difference of −0.1 ± 1.4 mm Hg.

Regional $\dot{V}_A/\dot{Q}$ ratios were used to create images of regional Se_{CO_2} or Pe_{CCO_2} (Fig. 6) for bronchoconstricted animals. These images showed fairly homogeneous distributions of Se_{CO_2} and Pe_{CCO_2} before bronchoconstriction. During bronchoconstriction there was marked heterogeneity in regional Se_{CO_2} and Pe_{CCO_2}, with regions of low Se_{CO_2} and low and high Pe_{CCO_2}.

DISCUSSION

In this study we demonstrate that functional information on $\dot{V}_A/\dot{Q}$ distributions derived from PET images of the lungs is quantitatively related to experimentally measured arterial blood gases. In spite of the limited spatial resolution of PET, the temporal information from the tracer kinetics data allows for the quantification of functionally important $\dot{V}_A/\dot{Q}$ heterogeneity within the imaging resolution.

PET has been used for assessment of regional distribution of $\dot{V}_A$, $\dot{Q}$, and $\dot{V}_A/\dot{Q}$ ratio in animal experiments (*14*) and human studies (*16*,*27*,*28*). The method of PET imaging after a bolus injection of ^{13}NN-saline has several advantages: (a) it is noninvasive and allows for in vivo measurements; (b) it provides higher resolution (~13 mm) than traditional planar nuclear medicine methods; (c) areas of shunt can be identified during the apneic period; (d) the total radiation dose to obtain $\dot{V}_A/\dot{Q}$ images of several lung regions is lower than that needed with a single CT slice; (e) $\dot{V}_A/\dot{Q}$ measurements can be obtained for a significant portion or all of the lung simultaneously in modern full body scanners; (f) it allows

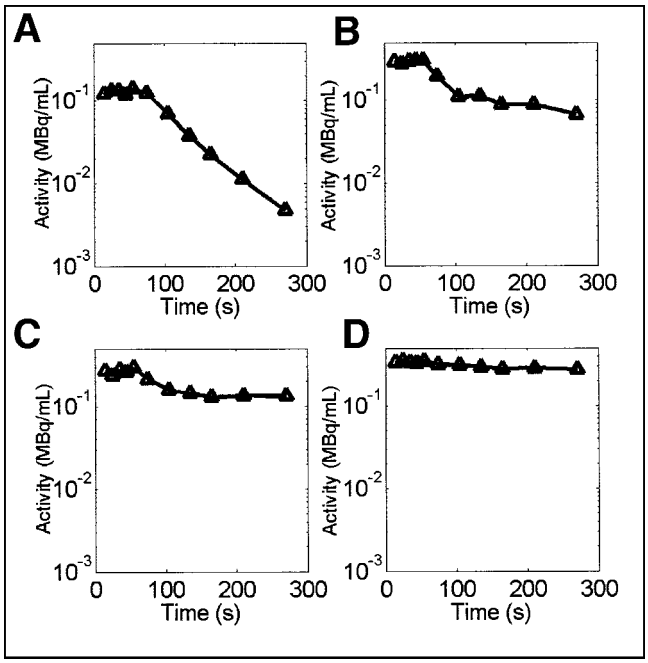

FIGURE 3. ^{13}NN washout curves in single examples of individual voxels for experimental data. (A) Normal, single-compartment region. (B) Intraregional heterogeneity suggesting 2-compartment washout. (C) Limit of heterogeneous condition when slow compartment essentially does not eliminate portion of tracer, corresponding to partial intraregional air trapping. (D) Region of virtually complete trapping where $\dot{V}_A \approx 0$. Since regional perfusion is finite, $\dot{V}_A/\dot{Q} \approx 0$.

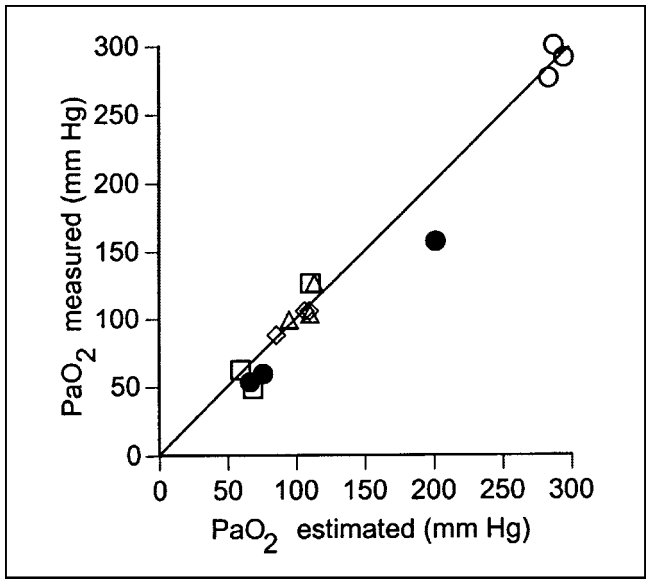

FIGURE 4. Measured vs. estimated global Pa_{O_2} derived from PET-based $\dot{V}_A/\dot{Q}$ distributions. Points correspond to values before (△) and after (◇) pulmonary embolism, after saline lung lavage (□), and before (○) and after (●) bronchoconstriction. Line of identity is shown for comparison.

for correlation with other functional and metabolic data in a single imaging session, given the short half-life of ^{13}NN; (g) because the tracer is delivered via the bloodstream, slow ventilating regions can be identified as trapped by their washout kinetics without the need for long equilibration periods. In relation to a technique with constant infusion of tracer, use of a bolus infusion minimizes corrections for tracer solubility in tissue and does not saturate the PET camera in areas of gas trapping.

Our results indicate that use of the ^{13}NN-saline injection technique can also accurately quantify regional and global gas exchange. This is a relevant finding because arterial blood gases are essential clinical tests for the evaluation of severity of gas exchange impairment and no current functional imaging technique has been shown to be predictive of global gas exchange. An imaging technique that provides simultaneously accurate topographic and quantitative functional information expands the ability for pathophysiologic investigation and diagnosis as indicated by studies applying quantitative lung scanning during pulmonary embolism (*5*) and chronic obstructive lung disease (*6*).

Assessment of intravoxel heterogeneity from temporal information was essential for accurate description of $\dot{V}_A/\dot{Q}$ distributions in disease states, such as acute lung injury with saline lung lavage and bronchoconstriction. In those states, the voxels showing subresolution heterogeneity represented a sizable fraction of the total imaged lung. This contrasts with the closely monoexponential washout seen in most voxels of normal lungs. This illustrates that the ^{13}NN-bolus injection PET imaging technique can quantitatively assess heterogeneity in regional $\dot{V}_A/\dot{Q}$ even when such heterogeneity occurs at length scales smaller than the camera resolution.

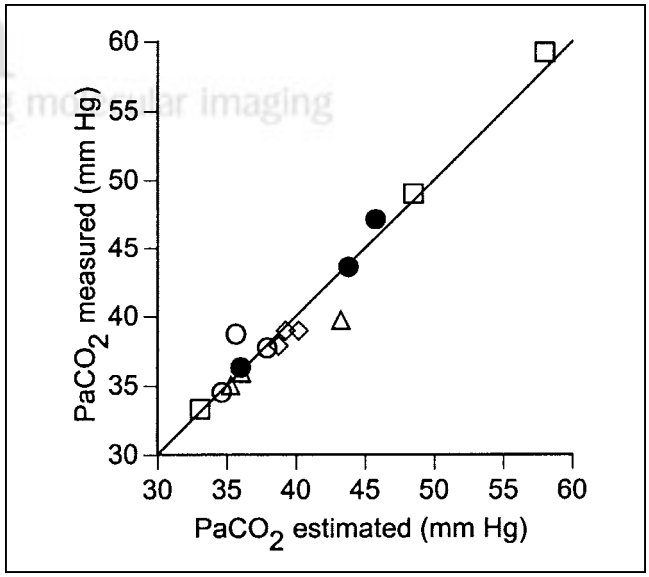

FIGURE 5. Measured vs. estimated global Pa_{CO_2} derived from PET-based $\dot{V}_A/\dot{Q}$ distributions. Points correspond to values before (△) and after (◇) pulmonary embolism, after saline lung lavage (□), and before (○) and after (●) bronchoconstriction. Line of identity is shown for comparison.

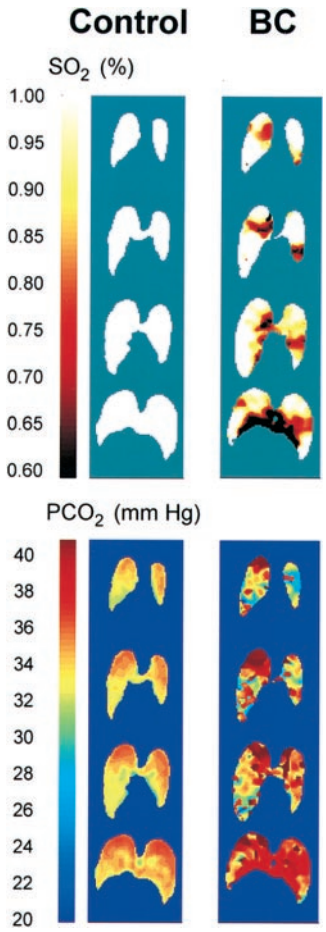

FIGURE 6. Maps of regional Sec_{O_2} and Pec_{CO_2} before (Control) and after bronchoconstriction (BC). Images are tomographic sections in craniocaudal direction from top to bottom. There is marked regional Sec_{O_2} (SO_2) and Pec_{CO_2} (PCO_2) heterogeneity after BC. Regional Pec_{CO_2} after BC shows larger degree of heterogeneity than Sec_{O_2}. Note different color scales for Sec_{O_2} and Pec_{CO_2} to best depict regional changes.

The spatial resolution achieved with PET is limited when compared with that of CT or MRI. Voxel size in our positron emission camera corresponds to $6.5 \times 6.5 \times 6$ mm, further filtered in our study to $13 \times 13 \times 13$ mm to reduce noise. This is significantly larger than the reported voxel size of $2.52 \times 2.52 \times 2.5$ mm for studies with CT (*10*) or $1.25 \times 1.25 \times 20$ mm for MRI (*29*). However, image noise was not studied in these methods and an ROI with >1,500 voxels was defined in the MRI study for quantitative estimates (*29*). The actual resolution needed to image detailed heterogeneity in lung function is not known. Perfusion heterogeneities can exist at dimensions as small as the acinar level (*30*). However, as resolution increases, the effect of lung motion artifacts is amplified and cross-registration errors compromise the results. Our results indicate that, despite not being able to visualize ventilation and perfusion at very small dimensions, PET can recover functionally significant $\dot{V}_A/\dot{Q}$ heterogeneity existing at length scales below the instrument's imaging resolution. This is because the temporal information contained in the PET scans can be used to estimate the effect of the intraresolution component of $\dot{V}_A/\dot{Q}$ heterogeneity.

Reconstruction artifacts are a potential problem of the PET technique. Since PET cameras are primarily designed for clinical applications, the selection of reconstruction algorithms is based on a balance of speed and quality of final results. Recently, improvements in reconstruction algorithms have been proposed (*31*) and could be applied for increased accuracy. Measurement noise in similar experimental settings was studied previously (*28,32*). Application of that analysis in our set of measurements indicates that ~6% of the perfusion variability in the original image is due to noise. Because of this, we spatially filtered the data to achieve a reduction of noise to <3%.

To estimate absolute regional $\dot{V}_A/\dot{Q}$ from the tracer kinetics we made the assumption that regional $s\dot{V}_r$ was proportional to regional ventilation $\dot{V}_r$. This assumption implicitly required that the volume of distribution of the injected tracer was equal in all perfused alveolar units. This assumption cannot be directly tested at this time. Although one could assign an alveolar gas volume to each voxel, based on the transmission scan, one would be neglecting the volume of conducting airways and the potential difference between voxel gas volume and the volume of distribution of the ^{13}NN tracer (*33*). Furthermore, it is not clear at present how to distribute such a volume among the subresolution compartments. The good matching between estimated and measured blood gases suggests that the assumed proportionality between $s\dot{V}_r$ and $\dot{V}_r$ is an acceptable approximation or at least one that does not create a systematic bias in our data.

Biologic variability is an unavoidable component of the measurements. The time lag between physiologic measurements and PET measurements was ~10 min. This should not have interfered with our calculations, given that steady-state conditions were maintained before initiating each set of measurements.

Actual ventilation of unperfused areas is not quantifiable with the current technique because the tracer is distributed by the pulmonary circulation. To specifically assess areas of very low or no perfusion, methods based on imaging the kinetics of inhaled tracer can be used (*14,17*). These very high to infinite $\dot{V}_A/\dot{Q}$ regions have more influence in the final determination of alveolar P_{CO_2}. O_2 exchange and, consequently, Pa_{O_2} will be more influenced by low $\dot{V}_A/\dot{Q}$ regions.

The volume of lung imaged in this study was limited to an axial field of 9.7 cm. Thus, the complete lung could not be assessed with a single scan sequence. Before imaging, positioning scans were reconstructed and the cross-sections of lung were selected to maximize the volume of imaged lung. We estimate that ~70% of the animal's lungs were imaged, providing a wide range of regional $\dot{V}_A$, $\dot{Q}$, and $\dot{V}_A/\dot{Q}$ values for analysis. Because the imaged lung was assumed in this work to characterize the whole lung, a large difference in the regional ventilation or perfusion between the imaged and nonimaged lung would compromise the agree-

ment between PET-estimated and directly measured blood gases. The fact that global results were closely matched suggests that both imaged and nonimaged lung had similar properties. Complete visualization of the lung with new-generation PET cameras eliminates this potential source of error. Alternatively, in cameras with smaller imaging field, >1 scan series can be done to image larger animals and humans.

$\dot{V}_A/\dot{Q}$ distributions obtained with PET were consistent with previous reports. For the prone normal sheep, $\dot{V}_A$- and $\dot{Q}$-weighted $\dot{V}_A/\dot{Q}$ distributions obtained with PET approximated a unimodal lognormal distribution, the typical distribution obtained in normal animals and humans using MIGET (*34*). $\dot{V}_A/\dot{Q}$ mismatch is increased after pulmonary embolism (*35*) and lung injury (*36*), and our estimates of $\dot{V}_A/\dot{Q}$ heterogeneity were always higher after pulmonary embolism and lung lavage. For bronchoconstricted animals, a clear bimodal distribution of perfusion was identified, in agreement with bimodal $\dot{V}_A/\dot{Q}$ distributions in experimental canine asthma (*37*) and in asthmatic humans (*38*).

Several imaging techniques have been used to evaluate regional ventilation and perfusion in the lungs. Initial studies used radiolabeled tracers and external radiation detectors (*3,4*). Planar scintigraphy of various radiopharmaceuticals plays an important role in the assessment of $\dot{V}_A/\dot{Q}$ in the lungs for diagnosis of pulmonary embolism (*39,40*) and estimate of pulmonary function after lung resection (*11*). The technique has restricted accuracy in the estimates of ventilation and perfusion and low spatial resolution. More recently, reports on the use of SPECT (*12*), CT (*10*), MRI (*8,9,29*), and PET (*14,16*) to estimate regional $\dot{V}_A/\dot{Q}$ have been presented. These methods afford advantages such as high spatial resolution and familiar, widely available technology. Kreck et al. (*10*) reported distributions of $\dot{V}_A/\dot{Q}$ obtained using xenon washin and CT. However, neither the obtained $\dot{V}_A/\dot{Q}$ distributions nor their result in terms of gas exchange were compared with any other independent method. The method uses a Xe inspired fraction of 65% and, because the tracer is delivered through inhalation, has low signal-to-noise ratios in low $\dot{V}_A/\dot{Q}$ units that are relevant to describe hypoxemia in disease. Eberle et al. (*29*) compared MRI estimates of alveolar P_{O_2} using inhaled hyperpolarized ^{3}He in large lung regions with end-tidal O_2 fraction measurements in normal pigs. The analysis was limited by the imaging of a single coronal slice, signal-to-noise ratio that implied use of large ROIs and interference of the measurement technique (delivery of ^{3}He) with the measured variable (alveolar P_{O_2}). Rhodes et al. (*15*) used a steady-state PET-based method to estimate $\dot{V}_A/\dot{Q}$ distributions in normal humans. Data were obtained from a single lung section and matched well previous concepts on ventrodorsal $\dot{V}_A/\dot{Q}$ gradient. These authors estimated SDs of $\dot{V}_A/\dot{Q}$ distributions but no comparison with independent methods to assess lung function was performed. Consequently, to date, no method for functional lung imaging has been shown to yield a quantitative measurement of gas exchange. Our method to estimate topographic distributions of $\dot{V}_A/\dot{Q}$ ratios produced measurements predictably related to global arterial blood gases and support the accuracy of the PET measurements.

Images of regional Sec_{O_2} and Pec_{CO_2} obtained from the estimates of regional $\dot{V}_A/\dot{Q}$ expanded the insight on regional gas exchange provided by the $\dot{V}_A/\dot{Q}$ information. This is because the relation between a given fractional distribution of $\dot{V}_A/\dot{Q}$ and Sec_{O_2} and Pec_{CO_2} is nonlinear and dependent on inspired gas fractions, total alveolar ventilation, CO, and hemoglobin concentration. Thus, extrapolation of a given regional $\dot{V}_A/\dot{Q}$ image to a regional Sec_{O_2} or Pec_{CO_2} image is not straightforward. The Sec_{O_2} and Pec_{CO_2} images provide the final result in terms of gas exchange of the regional $\dot{V}_A/\dot{Q}$ estimates for the specific physiologic and environmental conditions in study. In this work, the accuracy of the regional Sec_{O_2} and Pec_{CO_2} images is validated by their quantitative relation to measured arterial blood gases. It is unlikely in the severe disease states induced that the $\dot{V}_A/\dot{Q}$ distributions derived from regional PET measurements would be simultaneously predictive of global gas exchange and inaccurate at the regional level. The possibility of estimating regional respiratory gases makes the technique potentially applicable to the investigation of functional changes leading to gas transport impairment during lung disease and optimization of associated therapies.

In normal lungs there was a fairly homogeneous distribution of Sec_{O_2} and Pec_{CO_2} throughout the lung fields. This contrasts with the markedly heterogeneous distributions after bronchoconstriction. In these cases, images of Sec_{O_2} and Pec_{CO_2} showed substantial heterogeneity of the distribution of regional alveolar gas concentrations as a result of the increased $\dot{V}_A/\dot{Q}$ heterogeneity. The distribution of Pec_{CO_2} showed a larger degree of heterogeneity than that of Sec_{O_2}. These different regional distributions of Sec_{O_2} and Pec_{CO_2} reflect the distinct effects of $\dot{V}_A/\dot{Q}$ on regional blood gases depending on their gas partial pressure versus content relationship. Pec_{CO_2} decreases with increasing $\dot{V}_A/\dot{Q}$ from low $\dot{V}_A/\dot{Q}$ ($\sim$0.1) up to large $\dot{V}_A/\dot{Q}$ values. The regional image of Pec_{CO_2} consequently shows this continuous change of Pec_{CO_2} with $\dot{V}_A/\dot{Q}$ as $\dot{V}_A/\dot{Q}$ varies from 0.1 to 100. In contrast, because F_{IO_2} was kept around 50% in the bronchoconstricted animals, drops in Sec_{O_2} with $\dot{V}_A/\dot{Q}$ were seen only in areas of very low $\dot{V}_A/\dot{Q}$ ($<$0.1). Above a $\dot{V}_A/\dot{Q}$ of 0.1, end-capillary blood was close to complete saturation of hemoglobin and there was no observable change in Sec_{O_2} with $\dot{V}_A/\dot{Q}$.

CONCLUSION

We present a method to estimate regional $\dot{V}_A/\dot{Q}$ distributions and respiratory gas tensions based on regional tracer kinetics analysis of ^{13}NN imaged with PET. The analysis provides a quantitative assessment of $\dot{V}_A/\dot{Q}$ heterogeneity, including that corresponding to length scales smaller than the spatial resolution of the imaging method. The results are

consistent with those obtained with global methods—arterial blood gases and multiple inert-gas elimination technique—and indicate that estimates of regional $\dot{V}_A/\dot{Q}$ with the described method provide the advantage of being quantitatively predictive of global gas exchange.

ACKNOWLEDGMENTS

The authors thank Steven B. Weise and Sandra A. Barrow, PET Imaging Laboratory, Massachusetts General Hospital, for their expert support in the acquisition of images. This work was supported by the National Heart, Lung, and Blood Institute grant HL-56879.

REFERENCES

1. Lenfant C, Okubo T. Distribution function of pulmonary blood flow and ventilation-perfusion ratio in man. *J Appl Physiol.* 1968;24:668–677.
2. Wagner PD, Saltzman HA, West JB. Measurement of continuous distributions of ventilation-perfusion ratios: theory. *J Appl Physiol.* 1974;36:588–599.
3. Anthonisen NR, Dolovich MB, Bates DV. Steady state measurement of regional ventilation and perfusion ratios in normal man. *J Clin Invest.* 1966;45:1349–1356.
4. West JB. Pulmonary function studies with radioactive gases. *Annu Rev Med.* 1967;18:459–470.
5. Itti E, Nguyen S, Robin F, et al. Distribution of ventilation/perfusion ratios in pulmonary embolism: an adjunct to the interpretation of ventilation/perfusion lung scans. *J Nucl Med.* 2002;43:1596–1602.
6. Beydon L, Cinotti L, Rekik N, et al. Changes in the distribution of ventilation and perfusion associated with separation from mechanical ventilation in patients with obstructive pulmonary disease. *Anesthesiology.* 1991;75:730–738.
7. Kauczor HU, Hofmann D, Kreitner KF, et al. Normal and abnormal pulmonary ventilation: visualization at hyperpolarized He-3 MR imaging. *Radiology.* 1996;201:564–568.
8. Chen Q, Levin DL, Kim D, et al. Pulmonary disorders: ventilation-perfusion MR imaging with animal models. *Radiology.* 1999;213:871–879.
9. Kuethe DO, Caprihan A, Gach HM, Lowe IJ, Fukushima E. Imaging obstructed ventilation with NMR using inert fluorinated gases. *J Appl Physiol.* 2000;88:2279–2286.
10. Kreck TC, Krueger MA, Altemeier WA, et al. Determination of regional ventilation and perfusion in the lung using xenon and computed tomography. *J Appl Physiol.* 2001;91:1741–1749.
11. Jamadar DA, Kazerooni EA, Martinez FJ, Wahl RL. Semi-quantitative ventilation/perfusion scintigraphy and single-photon emission tomography for evaluation of lung volume reduction surgery candidates: description and prediction of clinical outcome. *Eur J Nucl Med.* 1999;26:734–742.
12. Palmer J, Bitzen U, Jonson B, Bajc M. Comprehensive ventilation/perfusion SPECT. *J Nucl Med.* 2001;42:1288–1294.
13. Mijailovich SM, Treppo S, Venegas JG. Effects of lung motion and tracer kinetics corrections on PET imaging of pulmonary function. *J Appl Physiol.* 1997;82:1154–1162.
14. Treppo S, Mijailovich SM, Venegas JG. Contributions of pulmonary perfusion and ventilation to heterogeneity in V_A/Q measured by PET. *J Appl Physiol.* 1997;82:1163–1176.
15. Rhodes CG, Valind SO, Brudin LH, Wollmer PE, Jones T, Hughes JM. Quantification of regional V/Q ratios in humans by use of PET. I. Theory. *J Appl Physiol.* 1989;66:1896–1904.
16. Rhodes CG, Valind SO, Brudin LH, et al. Quantification of regional V/Q ratios in humans by use of PET. II. Procedure and normal values. *J Appl Physiol.* 1989;66:1905–1913.
17. Vidal Melo MF, Harris RS, Layfield D, Musch G, Venegas JG. Changes in regional ventilation after autologous blood clot pulmonary embolism. *Anesthesiology.* 2002;97:671–681.
18. Stahl WR. Scaling of respiratory variables in mammals. *J Appl Physiol.* 1967;22:453–460.
19. Simon BA, Venegas JG. Analyzing ^{13}NN lung washout curves in the presence of intraregional nonuniformities. *J Appl Physiol.* 1994;76:956–964.
20. Wagner PD. Information content of the multibreath nitrogen washout. *J Appl Physiol.* 1979;46:579–587.
21. Galletti GG, Venegas JG. Tracer kinetic model of regional pulmonary function using positron emission tomography. *J Appl Physiol.* 2002;93:1104–1114.
22. Wagner PD, Hedenstierna G, Bylin G. Ventilation-perfusion inequality in chronic asthma. *Am Rev Respir Dis.* 1987;136:605–612.
23. Vidal Melo MF, Loeppky J, Caprihan A, Luft UC. Alveolar ventilation to perfusion heterogeneity and diffusion impairment in a mathematical model of gas exchange. *Comput Biomed Res.* 1993;26:103–120.
24. Sharan M, Popel AS. Algorithm for computing oxygen dissociation curve with pH, PCO_2, and CO in sheep blood. *J Biomed Eng.* 1989;11:48–52.
25. Loeppky JA, Luft UC, Fletcher ER. Quantitative description of whole blood CO_2 dissociation curve and Haldane effect. *Respir Physiol.* 1983;51:167–181.
26. Bland JM, Altman DG. Statistical methods for assessing agreement between two methods of clinical measurement. *Lancet.* 1986;327:307–310.
27. Schuster DP, Anderson C, Kozlowski J, Lange N. Regional pulmonary perfusion in patients with acute pulmonary edema. *J Nucl Med.* 2002;43:863–870.
28. Musch G, Layfield JD, Harris RS, et al. Topographical distribution of pulmonary perfusion and ventilation, assessed by PET in supine and prone humans. *J Appl Physiol.* 2002;93:1841–1851.
29. Eberle B, Weiler N, Markstaller K, et al. Analysis of intrapulmonary O_2 concentration by MR imaging of inhaled hyperpolarized helium-3. *J Appl Physiol.* 1999;87:2043–2052.
30. Glenny RW, Bernard SL, Robertson HT. Pulmonary blood flow remains fractal down to the level of gas exchange. *J Appl Physiol.* 2000;89:742–748.
31. Obi T, Matej S, Lewitt R, Herman G. 2.5-D simultaneous multislice reconstruction by series expansion methods from Fourier-rebinned PET data. *IEEE Trans Med Imaging.* 2000;19:474–484.
32. Winkler T, Harris RS, Musch G, Layfield J, Vidal Melo MF, Venegas JG. Length scale of heterogeneity in pulmonary blood flow (Q) and gas trapping (GT) in bronchoconstricted asthmatics [abstract]. *Am J Respir Crit Care Med.* 2002;165:A251.
33. O'Neill K, Venegas JG, Richter T, et al. Modeling kinetics of infused ^{13}NN-saline in acute lung injury. *J Appl Physiol.* 2003;95:2471–2484.
34. Wagner PD, Laravuso RB, Uhl RR, West JB. Continuous distributions of ventilation-perfusion ratios in normal subjects breathing air and 100 per cent O_2. *J Clin Invest.* 1974;54:54–68.
35. Santolicandro A, Prediletto R, Fornai E, et al. Mechanisms of hypoxemia and hypocapnia in pulmonary embolism. *Am J Respir Crit Care Med.* 1995;152:336–347.
36. Dantzker DR, Brook CJ, Dehart P, Lynch JP, Weg JG. Ventilation-perfusion distributions in the adult respiratory distress syndrome. *Am Rev Respir Dis.* 1979;120:1039–1052.
37. Rubinfeld AR, Wagner PD, West JB. Gas exchange during acute experimental canine asthma. *Am Rev Respir Dis.* 1978;118:525–536.
38. Wagner PD, Dantzker DR, Iacovoni VE, Tomlin WC, West JB. Ventilation-perfusion inequality in asymptomatic asthma. *Am Rev Respir Dis.* 1978;118:511–524.
39. Sostman HD, Coleman RE, DeLong DM, Newman GE, Paine S. Evaluation of revised criteria for ventilation-perfusion scintigraphy in patients with suspected pulmonary embolism. *Radiology.* 1994;193:103–107.
40. Gottschalk A, Sostman HD, Coleman RE, et al. Ventilation-perfusion scintigraphy in the PIOPED study. Part II. Evaluation of the scintigraphic criteria and interpretations. *J Nucl Med.* 1993;34:1119–1126.